

# Magneto-optical investigation of the field-induced spin-glass insulator to ferromagnetic metallic transition of the bilayer manganite $(\text{La}_{0.4}\text{Pr}_{0.6})_{1.2}\text{Sr}_{1.8}\text{Mn}_2\text{O}_7$

J. Cao,<sup>1,\*</sup> J. T. Haraldsen,<sup>2</sup> R. C. Rai,<sup>1</sup> S. Brown,<sup>1</sup> J. L. Musfeldt,<sup>1</sup> Y. J. Wang,<sup>3</sup> X. Wei,<sup>3</sup> M. Apostu,<sup>4,†</sup> R. Suryanarayanan,<sup>4</sup> and A. Revcolevschi<sup>4</sup>

<sup>1</sup>*Department of Chemistry, University of Tennessee, Knoxville, TN 37996*

<sup>2</sup>*Department of Physics and Astronomy, University of Tennessee, Knoxville, TN 37996*

<sup>3</sup>*National High Magnetic Field Laboratory, Florida State University, Tallahassee, FL 32310*

<sup>4</sup>*Laboratoire de Physico-Chimie de l'Etat Solide, UMR 8648 Batiment 414, Université Paris-Sud. F-91405 Orsay, France*

We measured the magneto-optical response of  $(\text{La}_{0.4}\text{Pr}_{0.6})_{1.2}\text{Sr}_{1.8}\text{Mn}_2\text{O}_7$  in order to investigate the microscopic aspects of the magnetic field driven spin-glass insulator to ferromagnetic metal transition. Application of a magnetic field recovers the ferromagnetic state with an overall redshift of the electronic structure, growth of the bound carrier localization associated with ferromagnetic domains, development of a pseudogap, and softening of the Mn-O stretching and bending modes that indicate a structural change. We discuss field- and temperature-induced trends within the framework of the Tomioka-Tokura global electronic phase diagram picture and suggest that controlled disorder near a phase boundary can be used to tune the magnetodielectric response. Remnants of the spin-glass insulator to ferromagnetic metallic transition can also drive 300 K color changes in  $(\text{La}_{0.4}\text{Pr}_{0.6})_{1.2}\text{Sr}_{1.8}\text{Mn}_2\text{O}_7$ .

PACS numbers: 78.20.Ls, 75.47.Lx, 71.30.+h, 75.50.Lk

## I. INTRODUCTION

Substituted perovskite manganites have attracted considerable attention due to their exotic magnetic, electronic, and optical properties. These properties derive from the many competing ground states of the complex phase diagram, strong coupling across different energy scales, and the presence of an inhomogeneous texture.<sup>1,2,3</sup> One consequence of this complexity is that enormous physical property changes can be induced by small chemical and physical perturbations. The double-layer manganites of interest here derive from the  $\text{La}_{1.2}\text{Sr}_{1.8}\text{Mn}_2\text{O}_7$  parent compound, crystallizing in a body-centered tetragonal structure (space group  $I4/mmm$ ) as shown in Fig. 1.<sup>4,5</sup> These bilayer manganites display a broad metallic regime, colossal magnetoresistance, Jahn-Teller distortions, metal-insulator transitions, and charge/orbital ordering.<sup>6,7,8</sup> These materials are therefore well-suited for fundamental magnetodielectric properties investigations.<sup>9,10,11,12,13,14,15,16,17,18,19,20,21,22,23</sup> They are also useful to extend the Tomioka-Tokura electronic phase diagram picture<sup>24</sup> and test oscillator strength sum rules.<sup>18,25</sup>

Pr substitution of the La sites in  $\text{La}_{1.2}\text{Sr}_{1.8}\text{Mn}_2\text{O}_7$  yields materials with chemical formula  $(\text{La}_{1-z}\text{Pr}_z)_{1.2}\text{Sr}_{1.8}\text{Mn}_2\text{O}_7$ , providing an opportunity to investigate the physical properties of bilayer manganites as a function of disorder without changing the total hole concentration.<sup>5</sup> Upon increasing Pr substitution ( $z=0, 0.2, \text{ and } 0.4$ ), the paramagnetic insulator (PMI) to ferromagnetic metal (FMM) transition temperature,  $T_c$ , decreases (120, 90, and 60 K, respectively).<sup>26</sup> At  $z=0.6$ , the transition is quenched.<sup>26</sup> This material,  $(\text{La}_{0.4}\text{Pr}_{0.6})_{1.2}\text{Sr}_{1.8}\text{Mn}_2\text{O}_7$ , is the subject of our present

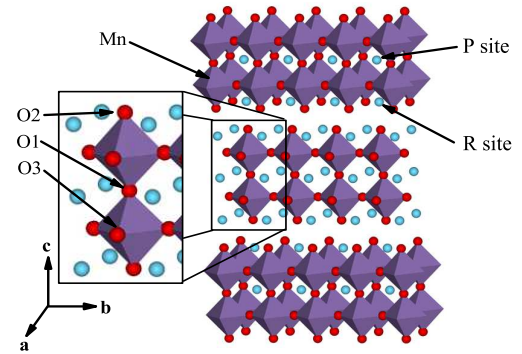


FIG. 1: (Color online) Crystal structure of  $(\text{La}_{0.4}\text{Pr}_{0.6})_{1.2}\text{Sr}_{1.8}\text{Mn}_2\text{O}_7$ , with O (red/black), Mn-containing octahedra (purple/gray), and the rare/alkaline earth ions (light blue/light gray). O occupies three different sites, and rare earth/alkaline earth metal have different coordination numbers depending on whether they occupy perovskite (P) or rock salt (R) sites.<sup>4,5</sup> Note that the unit cell along the  $b$  axis has been replicated to highlight the layered structure.

work. Pr substitution modifies the lattice constants ( $c/a$  increases), causes a change in the Jahn-Teller distortion, induces bound carrier localization in the far infrared, and modifies the  $e_g$  orbital occupancy.<sup>26,27,28</sup> Clearly, the degree of disorder strongly influences the physical properties. In fact, given that  $(\text{La}_{0.4}\text{Pr}_{0.6})_{1.2}\text{Sr}_{1.8}\text{Mn}_2\text{O}_7$  is highly disordered, the aforementioned low-temperature PMI state can likely be considered to be a spin-glass insulator (SGI) as well, although variable frequency ac susceptibility measurements are needed to confirm this

picture.<sup>5,24</sup>

The long-range ordered ferromagnetic state that is suppressed by chemical pressure in  $(\text{La}_{0.4}\text{Pr}_{0.6})_{1.2}\text{Sr}_{1.8}\text{Mn}_2\text{O}_7$  is recovered under magnetic field. This recovery is evident in the H-T phase diagram deduced from magnetization, magnetostriction, and resistivity measurements.<sup>29,30,31,32</sup> Neutron scattering demonstrates that the field-induced FMM state is very similar to the FMM state in the double-layer parent compound,  $\text{La}_{1.2}\text{Sr}_{1.8}\text{Mn}_2\text{O}_7$ .<sup>33</sup> Neutron diffraction studies show that local structure (Mn-O bond distances and Mn-O-Mn bond angles) and  $e_g$  orbital occupancies change dramatically in magnetic field, directly influencing electron hopping between Mn sites.<sup>27,34</sup> Magneto-optical imaging suggests that the high field FMM state is homogenous.<sup>35</sup>

In order to understand the interplay between spin, charge, lattice, and orbital degrees of freedom, we investigated the magneto-optical properties of  $(\text{La}_{0.4}\text{Pr}_{0.6})_{1.2}\text{Sr}_{1.8}\text{Mn}_2\text{O}_7$ . Application of a magnetic field recovers the ferromagnetic state with an overall redshift of the electronic structure, growth of the bound carrier localization associated with ferromagnetic domains, and softening of the Mn-O stretching and bending modes. The high field state is not, however, metallic in the conventional sense, and the spectrum differs from that of the double-layer parent compound  $\text{La}_{1.2}\text{Sr}_{1.8}\text{Mn}_2\text{O}_7$  in that it displays a pseudogap. We discuss field- and temperature-induced trends within the framework of the Tomioka-Tokura global electronic phase diagram picture<sup>24</sup> and suggest that controlled disorder near a phase boundary can be used to tune the magnetodielectric response. We also employ these microscopic changes to extract the H-T phase diagram and show that the low temperature lattice responds more slowly than spin and charge. Finally, we demonstrate that remnants of the SGI-FMM transition can drive 300 K color changes in  $(\text{La}_{0.4}\text{Pr}_{0.6})_{1.2}\text{Sr}_{1.8}\text{Mn}_2\text{O}_7$ .

## II. METHODS

Single crystals of  $(\text{La}_{0.4}\text{Pr}_{0.6})_{1.2}\text{Sr}_{1.8}\text{Mn}_2\text{O}_7$  were grown from sintered rods of same nominal composition by the floating-zone technique, using a mirror furnace.<sup>5</sup> Typical crystal dimensions were  $\approx 4 \times 5 \times 2$  mm<sup>3</sup>. They were cleaved to yield a shiny surface corresponding to the  $ab$  plane.

Near normal  $ab$  plane reflectance of  $(\text{La}_{0.4}\text{Pr}_{0.6})_{1.2}\text{Sr}_{1.8}\text{Mn}_2\text{O}_7$  was measured over a wide energy range (3.7 meV - 6.5 eV) using different spectrometers including a Bruker 113V Fourier transform infrared spectrometer, a Bruker Equinox 55 Fourier transform infrared spectrometer equipped with an infrared microscope, and a Perkin Elmer Lambda 900 grating spectrometer. The spectral resolution was 2 cm<sup>-1</sup> in the far and middle-infrared and 2 nm in the near-infrared, visible, and near-ultraviolet. Aluminum

mirrors were used as references for all measurements. Low temperature spectroscopies were carried out with a continuous-flow helium cryostat and temperature controller. Optical conductivity was calculated by a Kramers-Kronig analysis of the measured reflectance.<sup>36</sup>

The magneto-optical properties of  $(\text{La}_{0.4}\text{Pr}_{0.6})_{1.2}\text{Sr}_{1.8}\text{Mn}_2\text{O}_7$  were measured at the National High Magnetic Field Laboratory (NHMFL) in Tallahassee, FL, using a Bruker 113V Fourier transform infrared spectrometer equipped with a 18 T superconducting magnet and a grating spectrometer equipped with InGaAs and CCD detectors and a 33 T resistive magnet. Experiments were performed at 4.2 K for  $H \parallel c$ . Selected experiments were also carried out between 4.2 and 300 K in the spectral range of 0.75 - 3 eV. Data were collected on both increasing and decreasing magnetic field. Upsweep data were plotted here, whereas hysteresis effects on optical properties are discussed elsewhere.<sup>13</sup> After each field sweep, the samples were heated to 80 K to erase the “memory”. The field-induced changes in the measured reflectance were studied by taking the ratio of reflectance at each field and reflectance at zero field, i.e.,  $[R(H)/R(H=0 \text{ T})]$ . To obtain the high field optical conductivity, we renormalized the zero-field absolute reflectance with the high-field reflectance ratios, and recalculated  $\sigma_1$  using Kramers-Kronig techniques.<sup>36</sup> Due to limited coverage of the spectrometers at the NHMFL, the measured data were spliced together with curve fitting techniques between  $\sim 0.5$  and 0.75 eV.

We employed standard color rendering techniques to visualize temperature- and field-induced spectral changes.<sup>37,38</sup> Here, the absorption coefficient data<sup>39</sup> are “matched” with the effective absorption using a proportionality constant (which is typically on the order of the pellet thickness times the loading).<sup>40</sup> A comparison of the absorption coefficient to the effective absorption spectrum can be used to render color by integrating the product of the spectrum with the well-known XYZ color matching functions to determine the XYZ color values.<sup>37</sup> These XYZ values are converted into RGB color values and then inverted to determine the color of a material.<sup>37</sup> The final RGB values allow color rendering.

## III. RESULTS AND DISCUSSION

### A. Field Dependence of the Optical Spectra

Figure 2(a) displays the  $ab$  plane optical conductivity of  $(\text{La}_{0.4}\text{Pr}_{0.6})_{1.2}\text{Sr}_{1.8}\text{Mn}_2\text{O}_7$  in the low (SGI) and high field (FMM) states at 4.2 K. The dominant effect of the applied field is to redshift the oscillator strength, which is conserved within a few percent. A similar field-induced redshift of the spectral weight has been observed in other manganites.<sup>19,20,21,22</sup> In  $(\text{La}_{0.4}\text{Pr}_{0.6})_{1.2}\text{Sr}_{1.8}\text{Mn}_2\text{O}_7$ , the electronic excitation near 1 eV in the SGI state arises from a combination of Mn<sup>3+</sup> intra-atomic  $d$  to  $d$  ex-

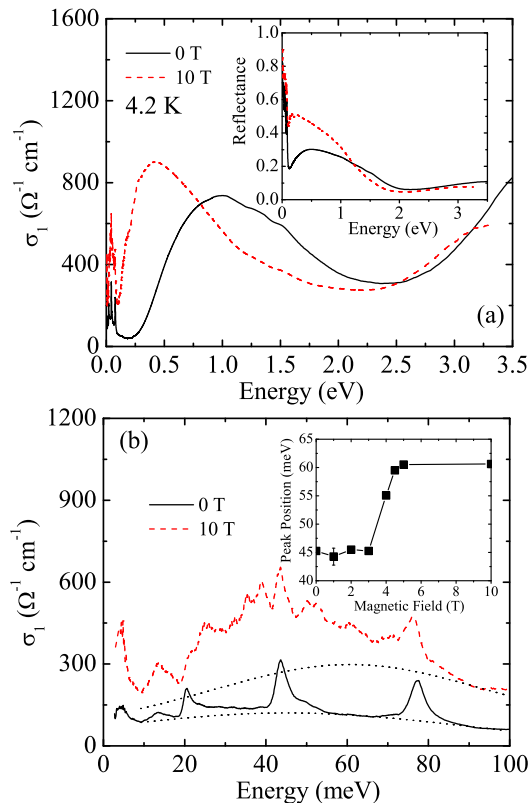


FIG. 2: (Color online) (a) Optical conductivity of  $(\text{La}_{0.4}\text{Pr}_{0.6})_{1.2}\text{Sr}_{1.8}\text{Mn}_2\text{O}_7$  within the  $ab$  plane under 0 (solid line) and 10 T (dashed line) at 4.2 K ( $H \parallel c$ ), extracted from a Kramers-Kronig analysis of the measured reflectance data (inset). (b) Close-up view of the 4.2 K optical conductivity within the  $ab$  plane under 0 and 10 T magnetic fields ( $H \parallel c$ ). Dotted lines guide the eye to highlight the broad underlying bound carrier localization. The inset shows the development of the bound carrier localization (dotted lines), associated with ferromagnetic domains, upon application of field.

citations superimposed with  $\text{Mn}^{3+}$  to  $\text{Mn}^{4+}$  ( $d$  to  $d$ ) inter-atomic charge transfer excitations.<sup>28,41,42</sup> This feature narrows and shifts to 0.4 eV in the high field FMM state. With increasing magnetic field, spectral weight also transfers to the lower energy region, enlarging the bound carrier excitation in the far infrared. This feature is a signature of ferromagnetic domain formation<sup>28</sup> and is discussed in more detail below. Note that the optical conductivity of  $(\text{La}_{0.4}\text{Pr}_{0.6})_{1.2}\text{Sr}_{1.8}\text{Mn}_2\text{O}_7$  does not show typical metallic behavior under any circumstances. Even at 10 T, where the system is driven into the FMM state, a far-infrared bound carrier excitation is observed rather than a Drude response. Manganites generally display low dc conductivities,<sup>1,2,3</sup> and  $(\text{La}_{0.4}\text{Pr}_{0.6})_{1.2}\text{Sr}_{1.8}\text{Mn}_2\text{O}_7$  is no exception. Transport measurements show that  $\sigma_{dc}$  is

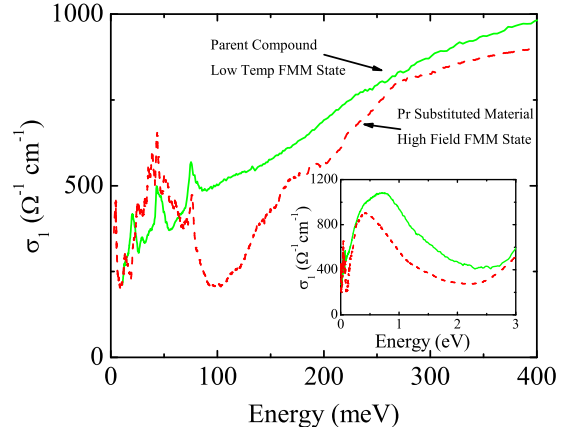


FIG. 3: (Color online)  $ab$  plane optical conductivity of the low temperature (10 K, 0 T) FMM state of  $\text{La}_{1.2}\text{Sr}_{1.8}\text{Mn}_2\text{O}_7$  and the high field (4.2 K, 10 T,  $H \parallel c$ ) FMM state of  $(\text{La}_{0.4}\text{Pr}_{0.6})_{1.2}\text{Sr}_{1.8}\text{Mn}_2\text{O}_7$ . The spectrum of the parent compound is from Ref. 42.

$\sim 10^{-5} \Omega^{-1} \text{cm}^{-1}$  in the low temperature insulating state and  $\sim 250 \Omega^{-1} \text{cm}^{-1}$  in the high field metallic state,<sup>29</sup> in reasonable accord with our optical properties data. The low-energy dielectric response, discussed below, is consistent with this picture.

Figure 2(b) displays a close-up view of the 4.2 K optical conductivity within the  $ab$  plane in zero (SGI) and high magnetic fields (FMM). Interestingly, the bound carrier excitation is stabilized in the high field state, moving from  $\sim 40$  to 60 meV with a substantial increase in oscillator strength. To quantify changes in localization with applied magnetic field, we fit the spectra with several model oscillators over this energy range. Both peak position (inset, Fig. 2(b)) and spectral weight show a first-order transition near 4 T, demonstrating that the ferromagnetic domains, which are associated with the bound carrier localization, couple to the field-induced transition. We previously conjectured that the presence of this low-energy bound carrier excitation in  $(\text{La}_{0.4}\text{Pr}_{0.6})_{1.2}\text{Sr}_{1.8}\text{Mn}_2\text{O}_7$  may be connected with the improved magnetoresistance properties.<sup>28</sup> Evidence for domains in the FMM state also comes from recent resistive relaxation studies.<sup>32</sup> Optical imaging techniques provide direct evidence for texture changes with applied magnetic field as well.<sup>35</sup>

To gain additional insight into the influence of disorder, it is useful to compare the low-energy dynamics in the field-induced FMM state of  $(\text{La}_{0.4}\text{Pr}_{0.6})_{1.2}\text{Sr}_{1.8}\text{Mn}_2\text{O}_7$  with the temperature-induced FMM state of the double-layer parent compound  $\text{La}_{1.2}\text{Sr}_{1.8}\text{Mn}_2\text{O}_7$ . The latter is obtained from the literature data of Lee *et al.*<sup>42</sup> Neither material is a conventional metal (Fig. 3). The optical conductivity of  $\text{La}_{1.2}\text{Sr}_{1.8}\text{Mn}_2\text{O}_7$  is characteristic of a weak metal, with a small polaron hopping band ( $\text{Mn}^{3+}$  to

Mn<sup>4+</sup> charge transfer) overlapping the onsite Mn *d* to *d* transitions.<sup>42</sup> The high-temperature  $\sim 0.15 - 0.3$  eV pseudogap in the optical conductivity is attributed to short-range charge/orbital ordering.<sup>42</sup> From a theoretical point of view, pseudogap formation is predicted to be a generic consequence of mixed-phase regimes.<sup>43</sup> This gap begins to fill below  $T_c$  and disappears in the low temperature FMM state.<sup>42</sup> The response of the Pr-substituted material is similar, but the far-infrared bound carrier excitation is separated from the asymmetric set of electronic excitations centered at 0.4 eV by a smaller pseudogap near 100 meV. The oscillator strength lost due to pseudogap formation is recovered in the bound carrier peak at 60 meV (Fig. 3). We conclude that, although the low temperature state of  $\text{La}_{1.2}\text{Sr}_{1.8}\text{Mn}_2\text{O}_7$  and the high field state of the Pr-substituted material are both considered to be FMMs from the bulk properties point of view,<sup>29,42</sup> their low-energy electronic response is different. In ARPES, *k*-space sampling is different and the pseudogap energy scale is more difficult to define because the gap is “soft”. Even so, in the high temperature phase, the size of the pseudogap is generally consistent with optical results in  $\text{La}_{1.2}\text{Sr}_{1.8}\text{Mn}_2\text{O}_7$  and related double layer manganites.<sup>42,44,45</sup> Interestingly, ARPES shows that the pseudogap persists into the low-temperature phase of  $\text{La}_{1.2}\text{Sr}_{1.8}\text{Mn}_2\text{O}_7$ , with an extrapolated value of  $\sim 90$  meV.<sup>46</sup> This differs from the optical property results for the parent compound below  $T_c$ ,<sup>42</sup> but is in line with the 100 meV pseudogap in  $(\text{La}_{0.4}\text{Pr}_{0.6})_{1.2}\text{Sr}_{1.8}\text{Mn}_2\text{O}_7$  (Fig. 3). Disorder effects in the Pr-substituted material likely break *k*-space selection rules and change the optical activity of this excitation.

Figure 4 displays the real part of the dielectric function, emphasizing the strong dielectric contrast between the low and high field states of

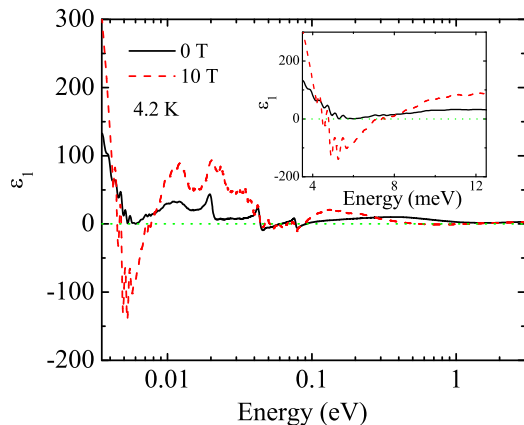


FIG. 4: (Color online) *ab* plane real part of the dielectric constant of  $(\text{La}_{0.4}\text{Pr}_{0.6})_{1.2}\text{Sr}_{1.8}\text{Mn}_2\text{O}_7$  at 4 K in the zero (SGI) and high field (FMM,  $H \parallel c$ ) states, as determined by Kramers-Kronig analysis.

( $\text{La}_{0.4}\text{Pr}_{0.6})_{1.2}\text{Sr}_{1.8}\text{Mn}_2\text{O}_7$ .<sup>47</sup> In the SGI state, the dispersive response is typical of a dielectric, with an overall positive  $\epsilon_1$  except for the strongest phonon dispersions. The dispersive response of the high field FMM state of the Pr-substituted compound is completely different. It first crosses zero at  $\sim 1.2$  eV, a plasma energy that is typical for a metal. However, it deviates from a Drude-like response and recrosses into positive territory at  $\sim 0.6$  eV. Below 0.01 eV,  $\epsilon_1$  turns sharply negative, indicative of weak metallic behavior, only to climb steeply below 4 meV. Multiple crossings of the dielectric function are reminiscent of metallic polymers, where competition between resonant quantum tunneling among nanoscale grains in the networks and variable range hopping processes determine the composite dielectric response.<sup>48</sup> The dielectric behavior of  $(\text{La}_{0.4}\text{Pr}_{0.6})_{1.2}\text{Sr}_{1.8}\text{Mn}_2\text{O}_7$  is very different from the field-induced dielectric change in  $\text{Nd}_{1/2}\text{Sr}_{1/2}\text{MnO}_3$  and  $\text{Pr}_{1/2}\text{Sr}_{1/2}\text{MnO}_3$ , where the three-dimensional FMM state is associated with a negative  $\epsilon_1$  in the low energy range.<sup>19,20</sup> Based upon the results of Fig. 4, we anticipate static magnetodielectric effects on the order of 100% in  $(\text{La}_{0.4}\text{Pr}_{0.6})_{1.2}\text{Sr}_{1.8}\text{Mn}_2\text{O}_7$ , although the mechanism may be very different from that in the low-bandwidth cubic manganite  $\text{Pr}_{0.7}\text{Ca}_{0.3}\text{MnO}_3$ , where the enormous magnetodielectric response at 100 Hz is attributed to a decrease in polaron activation energy with applied field.<sup>23,49</sup>

Direct information on how phonons couple with the magnetically driven transition in  $(\text{La}_{0.4}\text{Pr}_{0.6})_{1.2}\text{Sr}_{1.8}\text{Mn}_2\text{O}_7$  is also of interest, especially since stretching modes have been implicated in electronic kink formation in recent photoemission studies of a double-layer manganite,<sup>44</sup> and correlation between the Mn-O stretching mode and polaron formation was demonstrated by optics in  $\text{La}_{1.2}\text{Sr}_{1.8}\text{Mn}_2\text{O}_7$ .<sup>42</sup> In addition to the well-known infrared-active modes of the double-layer compounds,<sup>42</sup> the vibrational spectrum of  $(\text{La}_{0.4}\text{Pr}_{0.6})_{1.2}\text{Sr}_{1.8}\text{Mn}_2\text{O}_7$  exhibits a number of new, small modes in the low-field insulating state that are likely derived from the symmetry breaking effects of Pr substitution.<sup>28,50</sup> Some of these smaller structures become quite prominent in the FMM state, riding on top of the far-infrared bound carrier excitation (Fig. 2(b)). Several modes shift with applied field, indicative of a significant structural change between the low-field insulating to high-field metallic phases. Figure 5(a) displays trends in the field-dependent Mn-O stretching and bending modes. Upon increasing field, the 77.4 meV Mn-O(3) stretching mode softens on approaching to the transition, shows a sharp change through  $H_c$ , and saturates above 5 T. The 46.3 meV O-Mn-O bending mode is more complicated. It hardens on approaching the transition and then drops suddenly across  $H_c$ . Several other modes soften through the SGI - FMM transition as well, indicative of a structural change. For comparison, Fig. 5(b) displays the temperature dependent trends of the Mn-O stretching mode in both  $(\text{La}_{0.4}\text{Pr}_{0.6})_{1.2}\text{Sr}_{1.8}\text{Mn}_2\text{O}_7$  and  $\text{La}_{1.2}\text{Sr}_{1.8}\text{Mn}_2\text{O}_7$ .<sup>42</sup> Note

that the Mn-O stretching mode softens through  $T_c$  in the parent compound,<sup>42</sup> whereas it softens through  $H_c$  in the Pr-substituted material. We can also compare field-induced modifications in the Mn-O stretching and bending modes with neutron diffraction and magnetostriction results.<sup>34,51</sup> Neutron diffraction data shows that several bond lengths change with field. For instance, the distance between Mn and O(3) is 1.931(8) Å in the SGI state and increases to 1.937(2) Å in the FMM state.<sup>27,34</sup> This trend is consistent with our observation of softer phonon modes in the high field FMM state of  $(\text{La}_{0.4}\text{Pr}_{0.6})_{1.2}\text{Sr}_{1.8}\text{Mn}_2\text{O}_7$  (Fig. 5(a)). On the other hand, magnetostriction is a bulk technique. The elastic constants of  $(\text{La}_{0.4}\text{Pr}_{0.6})_{1.2}\text{Sr}_{1.8}\text{Mn}_2\text{O}_7$  soften through the transition and then tighten with applied field as Mn-O bond length disorder is suppressed.<sup>51</sup>

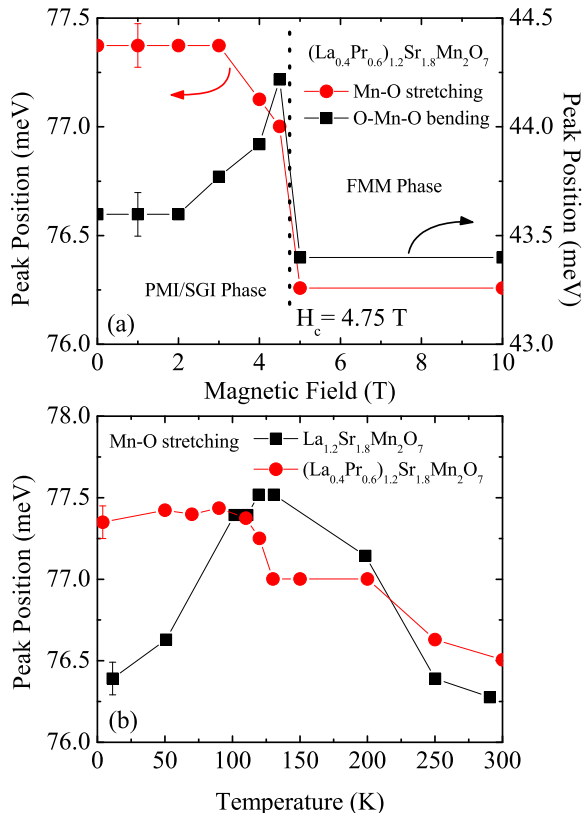


FIG. 5: (Color online) (a) Field-dependent Mn-O stretching and bending modes of  $(\text{La}_{0.4}\text{Pr}_{0.6})_{1.2}\text{Sr}_{1.8}\text{Mn}_2\text{O}_7$ . (b) Temperature-dependence of the Mn-O stretching modes of  $(\text{La}_{0.4}\text{Pr}_{0.6})_{1.2}\text{Sr}_{1.8}\text{Mn}_2\text{O}_7$  and  $\text{La}_{1.2}\text{Sr}_{1.8}\text{Mn}_2\text{O}_7$ , the double-layer parent compound ( $T_c=120$  K). Data for  $\text{La}_{1.2}\text{Sr}_{1.8}\text{Mn}_2\text{O}_7$  are from Lee *et al.* in Ref. 42.

Tomioka and Tokura recently proposed a global phase diagram of perovskite manganites within the plane of effective one-electron bandwidth and quenched disorder.<sup>24</sup>

TABLE I:

The averaged radii  $r_A$  and variance of the ionic radii  $\sigma^2$  of  $(\text{La}_{1-z}\text{Pr}_z)_{1.2}\text{Sr}_{1.8}\text{Mn}_2\text{O}_7$ , calculated at the perovskite (P) and rock salt (R) sites.

$z$	$T_c$ (K)	P Sites		R Sites	
		$r_A$ (Å)	$\sigma^2$ (Å <sup>2</sup> )	$r_A$ (Å)	$\sigma^2$ (Å <sup>2</sup> )
0	120	1.408	0.00154	1.272	0.00212
0.2	90	1.403	0.00226	1.269	0.00256
0.4	60	1.398	0.00294	1.266	0.00297
0.6	-	1.394	0.00358	1.264	0.00337

<sup>a</sup>The averaged radii  $r_A$  and the variance of the radii  $\sigma^2$  are calculated as  $r_A = \sum x_i r_i$  and  $\sigma^2 = \sum x_i (r_i^2 - r_A^2)$ , where  $x_i$  and  $r_i$  are the fractional occupancies ( $\sum x_i = 1$ ) and effective ionic radii of rare earth and alkaline earth cations, respectively.<sup>24,52</sup>

<sup>b</sup>Standard ionic radii are obtained from Refs. 55 and 56. The P site has a coordination number of 12, and the R site has a coordination number of 9.

These two parameters are controlled by the average value and the variance of rare earth and alkaline earth ionic radii, respectively. With increasing quenched disorder, the Y-shaped bicritical feature of the phase diagram splits and a SGI state emerges, separating the FMM and charge/orbital ordered antiferromagnetic phases. The authors propose that spin-glass character may enhance the colossal magnetoresistance effect in these materials.<sup>24</sup> Reviewing complexity in strongly correlated electronic systems, Dagotto emphasizes that this glassy region is dominated by short-range correlations and a local tendency towards either FMM or AFI regimes.<sup>53,54</sup>

Although the Tomioka-Tokura phase diagram was developed for cubic perovskites,<sup>24</sup> the underlying physics may be useful for understanding the double-layer manganites as well. We therefore investigated trends in  $(\text{La}_{1-z}\text{Pr}_z)_{1.2}\text{Sr}_{1.8}\text{Mn}_2\text{O}_7$  within the general framework of this global electronic phase diagram picture, modified to account for the two distinct perovskite (P) and rock salt (R) sites in the double-layer material. Table I shows calculated values of the averaged radii ( $r_A$ ) and the variance of the ionic radii ( $\sigma^2$ ) with different Pr substitution. Both P and R sites show the same trend:  $r_A$  decreases and  $\sigma^2$  increases with Pr substitution. Can we understand bulk property trends in  $(\text{La}_{0.4}\text{Pr}_{0.6})_{1.2}\text{Sr}_{1.8}\text{Mn}_2\text{O}_7$  within this picture? Table I shows the correlation between the PMI to FMM transition temperature ( $T_c$ ),<sup>5,26</sup> electronic bandwidth, and quenched disorder. With increasing Pr substitution,  $T_c$  decreases and is eventually quenched.<sup>5,26</sup> Despite the suppression of  $T_c$  at  $z=0.6$ ,  $(\text{La}_{0.4}\text{Pr}_{0.6})_{1.2}\text{Sr}_{1.8}\text{Mn}_2\text{O}_7$  is still in close proximity to the FMM phase boundary. Thus, a small local structure variation can modify  $r_A$  and  $\sigma^2$ , pushing the system back into the FMM state. The measured phonon softening through the  $H_c$  (Fig. 5(a)) demonstrates that local Mn-O bonding is more relaxed in the high field FMM state, in line with observations by Lee *et al.* of a relaxed lattice in the double-layer parent compound at low

temperature.<sup>42</sup> It is therefore probable that the applied field modifies  $r_A$  and overcomes substitution-induced disorder effects in  $\sigma^2$ , driving the system back into the FMM state in the Tomioka-Tokura phase diagram. The principal difference between the field-induced FMM state in  $(\text{La}_{0.4}\text{Pr}_{0.6})_{1.2}\text{Sr}_{1.8}\text{Mn}_2\text{O}_7$  and the temperature-induced FMM state in  $\text{La}_{1.2}\text{Sr}_{1.8}\text{Mn}_2\text{O}_7$  is the presence of the pseudogap in the substituted material (Fig. 3). The anticipated curvature of the SGI/FMM phase boundary in magnetic field is consistent with this picture and facilitates the magnetically-driven transition. At the same time, the low energy scale of  $H_c$  indicates the closely competing nature of the SGI and FMM phases in the Pr-substituted double-layer manganite. These results suggest that control of disorder in the proximity of a phase boundary may provide an important route to magnetodielectric materials that are switchable in low magnetic fields.

### B. Optical Phase Diagram

Our comprehensive magneto-optical measurements allow us to generate the H-T phase diagram of  $(\text{La}_{0.4}\text{Pr}_{0.6})_{1.2}\text{Sr}_{1.8}\text{Mn}_2\text{O}_7$  for  $H \parallel c$  (Fig. 6).<sup>57</sup> For comparison, we also plotted several points determined from selected resistivity, magnetization, and magnetostriction measurements.<sup>29,31,51</sup> Magnetization measurements indicate two boundaries at  $\sim 2$  and  $5$  T below  $50$  K, perhaps due to domain rotation.<sup>51</sup> Above  $50$  K, relaxation effects are more rapid.<sup>29</sup> Here, the phase diagram from both optics (which measures the microscopic nature of the charge degrees of freedom) and magnetization are in good agreement, although the boundary becomes more diffuse with increasing temperature (inset, Fig. 6(a)).

It is especially interesting to compare the correspondence of the low temperature phase boundaries in  $(\text{La}_{0.4}\text{Pr}_{0.6})_{1.2}\text{Sr}_{1.8}\text{Mn}_2\text{O}_7$ , determined by different techniques. Recently, Matsukawa *et al.* used combined resistivity, magnetization, and magnetostriction measurements to show that the bulk relaxation time of the lattice is two orders of magnitude smaller than that of the resistivity.<sup>32</sup> Extending this analysis to include microscopic trends, we find that the critical field extracted from field-induced changes in  $\text{Mn}^{3+} e_g$  orbital population is similar to the first magnetization boundary ( $\sim 2$  T). On the other hand, direct measurements of Mn-O and O-Mn-O stretching and bending vibrational modes (Fig. 5(a)) show excellent correspondence with critical fields determined from bulk magnetostriction, resistivity, and the second magnetization boundary ( $\sim 5$  T). Changes in the far-infrared bound carrier excitation (inset, (Fig. 2(b)) are also associated with this lattice distortion. The results demonstrate that the lattice responds more slowly than charge and spin over various length and time scales. The strong hysteresis in the low temperature physical properties<sup>5,13,29,31,32,51</sup> of  $(\text{La}_{0.4}\text{Pr}_{0.6})_{1.2}\text{Sr}_{1.8}\text{Mn}_2\text{O}_7$  derives from these differences.

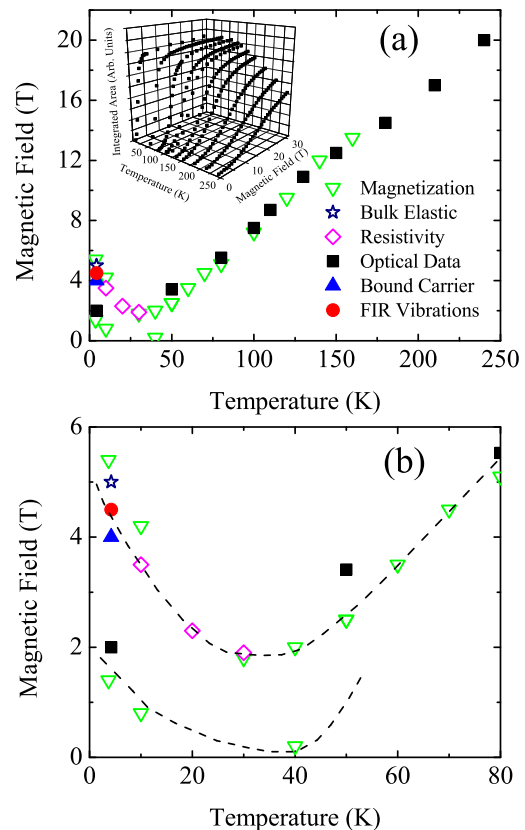


FIG. 6: (Color online) (a) H-T phase diagram, extracted from the optical properties data for  $H \parallel c$ . Data are taken with increasing field. Selected magnetization, magnetostriction, and resistivity results are shown for comparison.<sup>29,31,51</sup> The inset displays the absolute value of the integrated area of the reflectance ratio spectra in the color band region as a function of temperature and magnetic field. Inflection points in the data were used to determine phase boundary locations. (b) Close-up of view of the H-T phase diagram in the low temperature region.

### C. Field-Induced Color Changes at 300 K and Visualization

Controlled disorder near a phase boundary can clearly yield a substantial magnetodielectric response over a wide energy range. However, at this time, most magnetodielectric materials<sup>9,10,11,12,13,14,15,16,19,20,23</sup> display contrast only at low temperatures. Strategic control of spin-lattice interactions or the presence of a magnetically-driven phase transition (and associated change in ground state) offer potential routes to higher transition temperatures. The latter is investigated here. Specifically, we explored whether the remnants of the SGI-FMM transition in  $(\text{La}_{0.4}\text{Pr}_{0.6})_{1.2}\text{Sr}_{1.8}\text{Mn}_2\text{O}_7$  can be used to drive color property changes at room tem-

perature.

Figure 7 displays the room temperature optical conductivity of  $(\text{La}_{0.4}\text{Pr}_{0.6})_{1.2}\text{Sr}_{1.8}\text{Mn}_2\text{O}_7$  at 0 and 30 T. The field-induced spectral changes are similar to but smaller than those at base temperature (Fig. 2). Under applied magnetic field, the entire visible spectrum red-shifts. Given high enough magnetic field, the full SGI-FMM transition can likely be realized, inducing magneto-dielectric effects similar to those at 4 K. Recent  $^{139}\text{La}$  NMR studies reveal field-induced long-range ferromagnetic order up to 330 K in  $\text{La}_{1.2}\text{Sr}_{1.8}\text{Mn}_2\text{O}_7$ ,<sup>58</sup> suggesting that 300 K magneto-chromic effects may also be present in the parent compound.

We employed standard color rendering techniques to visualize the magneto-chromic and thermo-chromic effects in  $(\text{La}_{0.4}\text{Pr}_{0.6})_{1.2}\text{Sr}_{1.8}\text{Mn}_2\text{O}_7$  (Fig. 8).<sup>37,59</sup> Examination of the color panel shows a distinct color change between the 0 and 10 T data at low temperature, whereas there is only modest thermo-chromism as temperature is increased. The 300 K data taken at 30 T show a small change in color compared to that of the 0 T room temperature data. This shows that the color change is quenched by temperature although larger fields can probably drive the SGI to FMM transition at 300 K. In this case, we anticipate magneto-chromic effects similar to those at low temperature. The calculated RGB values are presented (Fig. 8) to quantify these color properties.

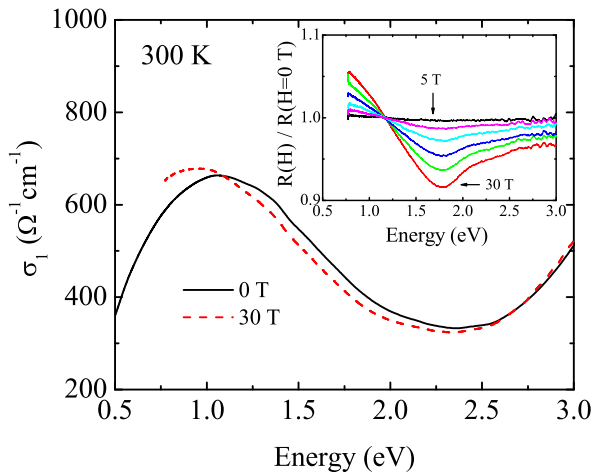


FIG. 7: (Color online) 300 K *ab* plane optical conductivity of  $(\text{La}_{0.4}\text{Pr}_{0.6})_{1.2}\text{Sr}_{1.8}\text{Mn}_2\text{O}_7$  in 0 T (solid line) and 30 T (dashed line) magnetic fields ( $H \parallel c$ ). The inset shows the measured *ab* plane reflectance ratio at 5, 10, 15, 20, 25, and 30 T (top to bottom). The data are taken upon increasing field.

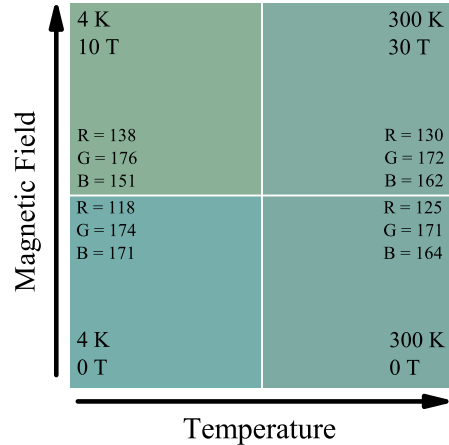


FIG. 8: (Color online) Schematic view of the temperature and magnetic field-induced color changes in  $(\text{La}_{0.4}\text{Pr}_{0.6})_{1.2}\text{Sr}_{1.8}\text{Mn}_2\text{O}_7$ . A comparison to transmittance data allows an estimated scaling constant of  $K=1.22 \times 10^{-5}$  cm to be determined. This K value was used in the calculation of the other colors. The RGB values for each swatch are given as well.

#### IV. CONCLUSION

We report a comprehensive magneto-optical investigation of  $(\text{La}_{0.4}\text{Pr}_{0.6})_{1.2}\text{Sr}_{1.8}\text{Mn}_2\text{O}_7$ , undertaken to examine the microscopic aspects of spin, lattice, charge, and orbital coupling through the SGI to FMM transition. Overall, spectral weight shifts to lower energy with applied magnetic field, although the material displays far-infrared localization and a pseudogap due to ferromagnetic domain formation and modest dc conductivity in the high field FMM state, different from that in the double-layer parent material. Several Mn-O and O-Mn-O stretching and bending vibrational modes soften through the field-driven transition, indicative of a structural change. Using the Tomioka-Tokura phase diagram picture<sup>24</sup>, we find that the FMM state, although quenched by chemical doping, is revived in a modified form by the application of magnetic field by driving the system from the disordered SGI phase into the FMM regime. The optical properties were also used to map the H-T phase diagram, and we find that the lattice response to the field is slower than that of spin and charge. Finally, we demonstrate that remnants of the SGI-FMM transition can drive 300 K color changes in  $(\text{La}_{0.4}\text{Pr}_{0.6})_{1.2}\text{Sr}_{1.8}\text{Mn}_2\text{O}_7$ . Color rendering provides a visual representation of the spectral changes. It is of future interest to complement this work with static magnetodielectric studies.

## V. ACKNOWLEDGMENTS

Work at the University of Tennessee is supported by the Materials Science Division, Basic Energy Sciences, U.S. Department of Energy (DE-FG02-01ER45885). The international aspects of this research were supported by

the National Science Foundation (INT-019650). A portion of this work was performed at the NHMFL, which is supported by NSF Cooperation Agreement DMR-0084173 and by the State of Florida. We thank E. Dagotto (UT/ORNL) and D. Dessau (Colorado) for useful discussions.

- 
- \* Electronic address: cao@ion.chem.utk.edu  
 † Permanent address: Al. I. Cuza University, Faculty of Chemistry, Physical, Theoretical and Materials Chemistry, Carol I, Iasi 700506 Romania
- <sup>1</sup> *Colossal Magnetoresistive Oxides*, edited by Y. Tokura (Gordon and Breach Science Publishers, New York, 2000).
  - <sup>2</sup> E. Dagotto, *Nanoscale Phase Separation and Colossal Magneto-resistance*, (Springer, 2003).
  - <sup>3</sup> *Colossal Magnetoresistive Manganites*, edited by T. Chatterji (Kluwer Academic Publishers, 2004)
  - <sup>4</sup> M. Kubota, H. Fujioka, K. Hirota, K. Ohoyama, Y. Moritomo, H. Yoshizawa, and Y. Endoh, *J. Phys. Soc. Jpn.* **69**, 1606 (2000).
  - <sup>5</sup> M. Apostu, R. Suryanarayanan, A. Revcolevschi, H. Ogasawara, M. Matsukawa, M. Yoshizawa, and N. Kobayashi, *Phys. Rev. B* **64**, 012407 (2001).
  - <sup>6</sup> Y. Moritomo, A. Asamitsu, H. Kuwahara, and Y. Tokura, *Nature (London)* **380**, 141 (1996).
  - <sup>7</sup> J. F. Mitchell, D. N. Argyriou, J. D. Jorgensen, D. G. Hinks, C. D. Potter, and S. D. Bader, *Phys. Rev. B* **55**, 63 (1997).
  - <sup>8</sup> T. G. Perring, G. Aeppli, Y. Moritomo, and Y. Tokura, *Phys. Rev. Lett.* **78**, 3197 (1997).
  - <sup>9</sup> C. dela Cruz, F. Yen, B. Lorenz, Y. Q. Wang, Y. Y. Sun, M. M. Gospodinov, and C. W. Chu, *Phys. Rev. B* **71**, R060407 (2005).
  - <sup>10</sup> B. Lorenz, A. P. Litvinchuk, M. M. Gospodinov, and C. W. Chu, *Phys. Rev. Lett.* **92**, 087204 (2004).
  - <sup>11</sup> T. Goto, T. Kimura, G. Lawes, A. P. Ramirez, and Y. Tokura, *Phys. Rev. Lett.* **92**, 257201 (2004).
  - <sup>12</sup> N. S. Rogado, J. Li, A. W. Sleight, and M. A. Subramanian, *Adv. Mater.* **17**, 2225 (2005).
  - <sup>13</sup> J. Choi, J. D. Woodward, J. L. Musfeldt, J. T. Haraldsen, X. Wei, M. Apostu, R. Suryanarayanan, and A. Revcolevschi, *Phys. Rev. B* **70**, 064425 (2004).
  - <sup>14</sup> J. Choi, J. D. Woodward, J. L. Musfeldt, X. Wei, M. H. Whangbo, J. He, R. Jin, and D. Mandrus, *Phys. Rev. B* **70**, 085107 (2004).
  - <sup>15</sup> J. D. Woodward, J. Choi, J. L. Musfeldt, J. T. Haraldsen, X. Wei, H. -J. Koo, D. Dai, M. -H. Whangbo, C. P. Landee, and M. M. Turnbull, *Phys. Rev. B* **71**, 174416 (2005).
  - <sup>16</sup> R. C. Rai, J. Cao, J. L. Musfeldt, D. J. Singh, X. Wei, R. Jin, Z. X. Zhou, B. C. Sales, and D. Mandrus, *Phys. Rev. B* **73**, 075112 (2006).
  - <sup>17</sup> H. J. Lee, K. H. Kim, M. W. Kim, T. W. Noh, B. G. Kim, T. Y. Koo, S.-W. Cheong, Y. J. Wang, and X. Wei, *Phys. Rev. B* **65**, 115118 (2002).
  - <sup>18</sup> A. S. Alexandrov and A. M. Bratkovsky, *J. Appl. Phys.* **87**, 5016 (2000).
  - <sup>19</sup> J. H. Jung, H. J. Lee, T. W. Noh, E. J. Choi, Y. Moritomo, Y. J. Wang, and X. Wei, *Phys. Rev. B* **62**, 481 (2000).
  - <sup>20</sup> J. H. Jung, H. J. Lee, T. W. Noh, Y. Moritomo, Y. J. Wang, and X. Wei, *Phys. Rev. B* **62**, 8634 (2000).
  - <sup>21</sup> Y. Okimoto, Y. Tomioka, Y. Onose, Y. Otsuka, and Y. Tokura, *Phys. Rev. B* **57**, R9377 (1998).
  - <sup>22</sup> Y. Okimoto, Y. Tomioka, Y. Onose, Y. Otsuka, and Y. Tokura, *Phys. Rev. B* **59**, 7401 (1999).
  - <sup>23</sup> R. S. Freitas, J. F. Mitchell, and P. Schiffer, *Phys. Rev. B* **72**, 144429 (2005).
  - <sup>24</sup> Y. Tomioka, and Y. Tokura, *Phys. Rev. B* **70**, 014432 (2004).
  - <sup>25</sup> A. S. Alexandrov and A. M. Bratkovsky, *Phys. Rev. B* **60**, 6215 (1999).
  - <sup>26</sup> M. Matsukawa, M. Narita, T. Nishimura, M. Yoshizawa, M. Apostu, R. Suryanarayanan, A. Revcolevschi, K. Itoh, and N. Kobayashi, *Phys. Rev. B* **67**, 104433 (2003).
  - <sup>27</sup> F. Wang, A. Gukasov, F. Moussa, M. Hennion, M. Apostu, R. Suryanarayanan, and A. Revcolevschi, *Phys. Rev. Lett.* **91**, 047204 (2003).
  - <sup>28</sup> J. D. Woodward, J. Choi, J. L. Musfeldt, J. T. Haraldsen, M. Apostu, R. Suryanarayanan, and A. Revcolevschi, *Phys. Rev. B* **69**, 104415 (2004).
  - <sup>29</sup> I. Gordon, P. Wagner, V. V. Moshchalkov, Y. Bruynseraede, M. Apostu, R. Suryanarayanan, and A. Revcolevschi, *Phys. Rev. B* **64**, 092408 (2001).
  - <sup>30</sup> P. Wagner, I. Gordon, V. V. Moshchalkov, Y. Bruynseraede, M. Apostu, R. Suryanarayanan, and A. Revcolevschi, *Europhys. Lett* **58**, 285 (2002).
  - <sup>31</sup> M. Matsukawa, M. Chiba, A. Akasaka, R. Suryanarayanan, M. Apostu, A. Revcolevschi, S. Nimori, and N. Kobayashi, *Phys. Rev. B* **70**, 132402 (2004).
  - <sup>32</sup> M. Matsukawa, K. Akasaka, H. Noto, R. Suryanarayanan, S. Nimori, M. Apostu, A. Revcolevschi, and N. Kobayashi, *Phys. Rev. B* **72**, 064412 (2005).
  - <sup>33</sup> F. Moussa, M. Hennion, F. Wang, A. Gukasov, R. Suryanarayanan, M. Apostu, and A. Revcolevschi, *Phys. Rev. Lett.* **93**, 107202 (2004).
  - <sup>34</sup> A. Gukasov, F. Wang, B. Anighofer, L. He, R. Suryanarayanan, and A. Revcolevschi, *Phys. Rev. B* **72**, 092402 (2005).
  - <sup>35</sup> Y. Tokunaga, M. Tokunaga, and T. Tamegai, *Phys. Rev. B* **71**, 012408 (2005).
  - <sup>36</sup> F. Wooten, *Optical Properties of Solids* (Academic Press, New York, 1972).
  - <sup>37</sup> F. W. Billmeyer and M. Saltzman, *Principles of Color Technology, 3rd Ed.*, Wiley, New York (2000).
  - <sup>38</sup> J. L. Musfeldt, D. B. Tanner, and A. J. Paine, *J. Opt. Soc. Am. A* **10** 2648 (1993).
  - <sup>39</sup> Through a Kramers-Kronig analysis, one can determine the extinction coefficient as a function of frequency,  $\kappa(\omega)$ . The absorption coefficient,  $\alpha$ , is calculated as  $\alpha=4\pi\kappa(\omega)$ .
  - <sup>40</sup> The absorption coefficient needs to be normalized by a constant, K, to determine the effective absorption of the material. K is dependent on factors such as the mass fraction and thickness of the transmittance sample. However, because these are reflectance measurements of a solid ma-



- terial,  $K$  is unknown. This constant can be approximated by an examination of the transmittance of the material or by normalizing the absorption to a distinct value of color (assuming the color of the material is known). Once  $K$  is determined for a material, it is the same for all spectra and is not dependent on magnetic field or temperature.
- <sup>41</sup> T. Ishikawa, T. Kimura, T. Katsufuji, and Y. Tokura, *Phys. Rev. B* **57**, R8079 (1998).
- <sup>42</sup> H. J. Lee, K. H. Kim, J. H. Jung, T. W. Noh, R. Suryanarayanan, G. Dhalenne, and A. Revcolevschi, *Phys. Rev. B* **62**, 11320 (2000).
- <sup>43</sup> A. Moreo, S. Yunoki, and E. Dagotto, *Phys. Rev. Lett.* **83**, 2773 (1999).
- <sup>44</sup> Z. Sun, Y. -D Chuang, A. V. Fedorov, J. F. Douglas, D. Reznik, F. Weber, N. Aliouane, D. N. Argyriou, H. Zheng, J. F. Mitchell, T. Kimura, Y. Tokura, A. Revcolevschi, and D. S. Dessau, arXiv:cond-mat/0510255 v1, 10 Oct 2005.
- <sup>45</sup> N. Mannella, W. L. Yang, X. J. Zhou, H. Zheng, J. F. Mitchell, J. Zaanen, T. P. Devereaux, N. Nagaosa, Z. Husain, and Z.-X. Shen, *Nature* **438**, 474 (2005).
- <sup>46</sup> Y.-D. Chuang, A. D. Gromko, D. S. Dessau, T. Kimura, and Y. Tokura, *Science* **292**, 1509 (2001).
- <sup>47</sup> In contrast,  $\epsilon_1$  of the parent compound in the FMM state is positive within the whole frequency range, increasing upon approaching to zero energy, following a typical “bad metal” behavior.<sup>42</sup>
- <sup>48</sup> V. N. Prigodin and A. J. Epstein, *Physica B: Condensed Matter* **338**, 310 (2003).
- <sup>49</sup> This is because the polaron excitation remains well-defined in the high field FMM state of  $(\text{La}_{0.4}\text{Pr}_{0.6})_{1.2}\text{Sr}_{1.8}\text{Mn}_2\text{O}_7$  (Fig. 2(a)).
- <sup>50</sup> D. B. Romero, V. B. Podobedov, A. Weber, J. P. Rice, J. F. Mitchell, R. P. Sharma, and H. D. Drew, *Phys. Rev. B* **58**, R14737 (1998).
- <sup>51</sup> Y. Nakanishi, K. Shimomura, T. Kumagai, M. Matsukawa, M. Yoshizawa, M. Apostu, R. Suryanarayanan, A. Revcolevschi, and S. Nakamura, (unpublished).
- <sup>52</sup> L. M. Rodriguez-Martinez and J. P. Attfield, *Phys. Rev. B* **54**, R15622 (1996).
- <sup>53</sup> J. Burgy, M. Mayr, V. Martin-Mayor, A. Moreo, and E. Dagotto, *Phys. Rev. Lett.* **87**, 277202 (2001).
- <sup>54</sup> E. Dagotto, *Science* **309**, 257 (2005).
- <sup>55</sup> E. Pollert, S. Krupička, and E. Kuzmíčová, *J. Phys. Chem. Solids* **43**, 1137 (1982).
- <sup>56</sup> R. D. Shannon, *Acta Crystallogr. Sec. A* **32**, 751 (1976).
- <sup>57</sup> We measured the magneto-optical response of  $(\text{La}_{0.4}\text{Pr}_{0.6})_{1.2}\text{Sr}_{1.8}\text{Mn}_2\text{O}_7$  as a function of temperature and field, and quantified the changes by plotting the absolute value of the integrated intensities of the field-induced feature. The first derivative of this change determined the boundary from the optical perspective.
- <sup>58</sup> Y. Shiotani, J. L. Sarrao, and Guo-qing Zheng, *Phys. Rev. Lett.* **96**, 057203 (2006).
- <sup>59</sup> In the calculation of color, the 300 K (0 T) data were normalized to  $K=1.22\times 10^{-5}$  cm,<sup>40</sup> chosen by a comparison to room temperature transmittance. The same value of  $K$  was used to normalize the other data, allowing us to compare overall color changes to those of the 300 K, zero field data.